Comparative Analysis of Turbulent Plane Jets from a Sharp-Edged Orifice, a Beveled-Edge Orifice and a Radially Contoured Nozzle

Ravinesh C. Deo

Abstract—This article investigates through experiments the flow characteristics of plane jets from sharp-edged orifice-plate, beveled-edge and radially contoured nozzle. The first two configurations exhibit saddle-backed velocity profiles while the third shows a top-hat. A vena contracta is found for the jet emanating from orifice at $x/h \approx 3$ while the contoured case displays a potential core extending to the range $x/h = 5$. A spurt in jet pressure on the centerline supports vena contracta for the orifice-jet. Momentum thicknesses and integral length scales elongate linearly with x although the growth of the shear-layer and large-scale eddies for the orifice are greater than the contoured case. The near-field spectrum exhibits higher frequency of the primary eddies that concur with enhanced turbulence intensity. Importantly, highly "turbulent" state of the orifice-jet prevails in the far-field where the spectra confirm more energetic secondary eddies associated with greater flapping amplitude of the orifice-jet.

Keywords—Orifice, beveled-edge-orifice, radially contoured nozzle, plane jets.

I. INTRODUCTION

THE study of a turbulent plane jet continues in research arena since pioneer investigations of Schlichting [1]. A primary reason is the jet's statistically two-dimensional nature, which is advantageous for applications in numerical modeling and the understanding of jet propulsion, airlifting, combustion, ventilation and environmental fluidic systems [2], [3]. Within the analytical, experimental and computational domains, plane jets efflux through a slender (rectangular) slot with exit dimensions $w \times h$, where $w \gg h$, and the nozzle is bounded by sidewalls attached to the h side of the slot. The sidewalls enhance statistical two-dimensionality up to a downstream location that depends on the aspect ratio, $AR = w/h$ [4].

Three alternative geometric configurations commonly used are the sharp-edged (*orifice*) plate with 45° beveled or straight-cut abrupt edge [5], smoothly contracting (*contoured*) nozzle with a sinusoidal curvature profile [6], [7] and *radially contracting* nozzle with a contracting exit of a reasonably large radius of curvature (r), where $r \gg h$ [8], [9] The first configuration produces a "saddle-backed" mean exit profile, while the other two a ''top hat'' with laminar exit conditions. However, the orifice and radially contracting geometries are much easier to design and manufacture than smooth contraction nozzles, especially when the shape is non-circular. The radially

contracting nozzle also hails with the added advantage of being able to be modified easily (e.g. reducing the radius of curvature to achieve a beveled-edge-orifice) [10]. By comparison, only a few studies have employed an orifice or a beveled-edge-orifice, perhaps due to the near-field flow being far more complex (e.g. presence of a vena contracta) or for reasons otherwise. Similarly, the radially contoured nozzle has also not been researched since its first inception by [8] and more recently by [10]. Hence, the present investigation broadens the understanding of the jet flows emanating from these two configurations.

Over past decades, there has been increasing evidence that the effects of the differences in upstream (jet-exit) conditions propagate downstream even into the far field, self-preserving region [11]–[14]. An extensive search of published literature on jets issuing from orifice and contoured configurations reveals voluminous information on the flow field of round or pipe jets [14]–[16] and of rectangular or elliptic jets [17] although there is a paucity of data on plane jets. However, considering the broad similarity between rectangular and plane jets, especially in the near field where the two are considered statistically two-dimensional [18], we may interpret the nature of the emerging flow structure of plane jets based on investigations conducted on the rectangular jets. For instance, the study of Quinn [17] of a jet issuing from a sharp-edged elliptic orifice plate and elliptic contoured nozzle showed that the mixing rates of the orifice were higher that of the contoured nozzle. It was not until recently that a direct comparison of the statistical properties of plane jets of different nozzle geometric configurations was undertaken [10]. The study found a higher formation rate of large-scale, coherent vortices in the near field, greater jet spreading and decaying rates of mean centerline velocity and a larger magnitude of the asymptotic turbulence intensity for the orifice. In totality, the primary statistical properties could inject secondary effects into the self-preserving field to modify the large and small-scale flow structures and the corresponding turbulent mixing behaviors of the propagated jet [19]. However, no definite deduction about flow structures of plane jets from the orifice and contoured nozzle is currently available, which forms the basis of the present investigation.

Accordingly the present study focuses on the following (1) to conduct a direct comparison of the flow characteristics of jets issuing from a sharp-edged orifice plate, a beveled-edge-orifice and a radially contoured nozzle, (2) to explore the physical mechanisms responsible for any differences identified in the

Dr RC Deo is with the School of Agricultural, Computational and Environmental Sciences at University of Southern Queensland (Springfield), Australia (phone: +61(07) 38078861; fax: +61(07) 38078861; correspondence e-mail: ravinesh.deo@usq.edu.au).

comparison of these jets. To meet the needful, single hot-wire measurements are employed to measure the mean and turbulent properties of the three jets issuing from a large aspect ratio nozzle (AR = 72), measured at a Reynolds number of 18 000 throughout the near and far fields. The differences in the underlying flow structure are quantified by spectral, autocorrelation and probability density analysis of the instantaneous velocity recorded over the range $0 \leq x/h \leq 85$.

II. EXPERIMENTAL DESIGN

A. Jet Facility and Nozzle Parameters

The present experiments were conducted in the fluid mechanics laboratory within the School of Mechanical Engineering, University of Adelaide. Full details of the experimental setup are stated in [10]–[14] so that only a brief description with the overall schematic view is shown in Fig. 1. The jet facility consists of a variable-speed 14.5 kW aerofoil-type centrifugal fan, pre-conditioned by a wide-angle diffuser, settling chamber, honeycombs, and screens that feed air of uniform flow into a polynomial contraction plenum. The exit dimensions of the plenum was w = 340mm and l = 720mm, where the three plane nozzles were attached. Filtered and compressed air was supplied through the plenum into the nozzle, with a pair of sidewalls aligned along the long side of the contraction to enhance two-dimensionality of the plane jet.
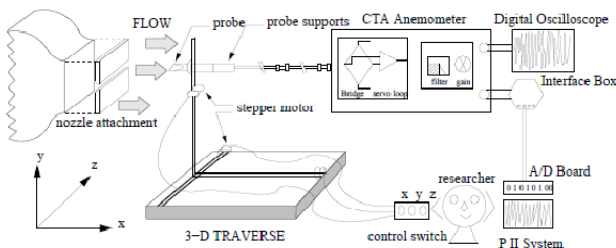

Fig. 1 The experimental scheme showing the present nozzle attachment to the wind tunnel exit, hot wire and data acquisition systems (Reproduced after [14])

The plane nozzles were made from a pair of three flat plates, with a slot opening height (h) = 10mm to produce a large-aspect ratio nozzle (AR = w/h) of 72. The first nozzle was a sharp-edged type ("termed hereafter as the *orifice plate*") designed with an abrupt corner edge along the long-sides facing upstream, the second with radially contracting long-sides of exit radii (r) = 45mm ("*beveled-edge-orifice*"), and the third whose r = 360mm ("*radially contoured*"). While the former nozzle resembled the beveled edge, true orifice plate that produces a saddle-backed, mean profile [5], the latter, according to our previous findings [10] produced a mean velocity profile that was approximately uniform to closely match the conventional smoothly contoured nozzle used in previous investigations [6], [7]. For all the three jets, the Reynolds number $Re_h \equiv U_b h/\upsilon$ is nominally set to $(1.80 \pm 0.20)\times10^4$, where U_b is the bulk mean exit velocity through the nozzle exit and υ is the kinematic viscosity of the isothermal air,

with the Mach number M = U_b/c = 0.08 (c being the speed of sound).

B. Hot Wire Measurements

A constant temperature anemometer (CTA) employing single hot-wire probes has been used to undertake velocity measurements within the present plane jets. Following [19], custom-designed copper-plated tungsten hot-wire sensors of suitable configuration were chosen to minimize thermal decay from the ends of the probe and to resolve small-scale turbulence structures. The length of the probe, l_w and diameter d_w of the probe has been chosen based on previous work. According to [20], the heat losses from the probe is $\approx$15% when the ratio $l_w/d_w \approx 200$ and the sensor is operated at an overheat ratio greater than 1.0. In the present work, $l_w \approx$1 mm and d_w = 5μm, so that $l_w/d_w \approx 200$, which is sufficient to dampen the low-frequency attenuation of the signal [21]. The overheat ratio of the CTA was set to 1.5 in order to minimize heat losses from the ends of the probe.

Prior to each measurement, the total jet pressure (hence the corresponding velocity U) was measured using a Pitot static tube to determine a suitable transfer function to be used for calibrating the probe. In the present experiment, a fourth order polynomial-type transfer function of the form, $U = C_0 + C_1 V + C_2 V^2 + C_3 V^3 + C_4 V^4$ (where C_0, C_1... C_4 are experimental constants) is chosen instead of the King's Law, as it is considered less accurate, particularly in larger turbulence intensity flows [19]. The calibrations have been performed within the jet's potential core, where the turbulence intensity was less than 0.5%. For greater accuracy, two sets of calibrations have been performed, one before and one after each experiment to determine the observed drifts in flow velocity due to changes in ambient conditions or other random uncertainties. Given the controlled laboratory environment with isothermal conditions, very small occasional drifts in calibrated velocity or $U \pm 1.5\%$ have been noted. These are compensated by repeating the particular measurement, or using an 'average' transfer function of the two sets of calibrations, depending on the magnitude of the velocity drift.

A three-dimensional traverse system enabled measurements laterally (across the y-direction of the jet or the shear layers) and axially (in the x-direction or the main free-stream flow). For the present velocity measurements, a *PC-30F* data acquisition system hooked to a personal computer, with a 200 kHz multi-channel analogue to digital converter with a 2.4 mV resolution enhanced by a FIFO buffer is utilized. The system incorporated programmable gain that made it ideal for measuring low-level signals. The instantaneous velocity signal was monitored on a Digital Tektronix Oscilloscope and data were visualized in WaveView 2.0 for preliminary inspection and frequency analysis. The input range of input board was $\pm$ 5.0 V, so an appropriate offset was applied to the sampled voltage to rectify the signal within the $\pm$ 3.0 V. This avoided clipping the tails of higher order moments of velocity fluctuations, as stipulated by [22]. The signals were filtered at a cut-off frequency (f_c) = 9.2 kHz chosen to eliminate high-frequency noise and sampled at a Nyquist frequency f_n =

$2f_c$ = 18.4 kHz .The data record duration was 22.4 s, in which the 400 000 data points were collected, that are considered sufficient for spectral analysis of the flow structure.

The present experimental uncertainties in the mean and rms values of temperature and velocity are estimated based on the inaccuracies in the calibration process and observed scatter in the measurements. The estimated percentage uncertainties are: mean error of ± 4% for lateral velocity measurements and ±0.8% for the centerline, and the centerline mean velocity error of ±0.8%, root-mean-square (rms) velocity ±1.8% respectively. The mean error in the integral quantity is estimated to be ±10%.

TABLE I
NOZZLE-EXIT CONDITIONS FOR THREE JETS

Initial Parameters	Sharp-edged Orifice	Beveled edge	Radially Contoured
Displacement Thickness, δ_d	-	0.0054h	0.151h
Momentum Thickness, θ_m	-	0.0030h	0.061h
Shape Factor, $H = \delta_m / \theta_m$	-	1.80	2.48
Momentum-based Reynolds Number, $Re_{\theta m} = U_b \theta_m / \upsilon$	-	55	112
Centerline Turbulence Intensity, u'_c / U_c (%)	3.0	2.5	1.50
Peak-shear Layer Turbulence Intensity, u'_p / U_c (%)	22.0	17.0	4.0
Turbulence Reynolds Number, $Re_{u'} = u'_p h / \upsilon$	4040	3122	734

III. RESULTS AND DISCUSSION

A. Initial (or Exit) Conditions

The measurement of the lateral distribution of mean and fluctuating velocity close to the exit for the beveled-edge-orifice and contoured nozzle, also reported previously in [10] revealed dramatic dependence of initial conditions on the nozzle type. The orifice-plate produced a clearly defined, saddle-backed mean exit profile, which typifies the presence of a vena contracta in the immediate near field flow. The presence of the vena contracta is broadly consistent with a number of previous investigations on orifice-jets [12], [13], [16], [17]. The present beveled-edge nozzle also produced a similar saddle-backed profile; however, the magnitude of velocity deficit was smaller than that of the orifice-plate, suggesting that the vena contracta was somewhat suppressed for this case. Unlike these two nozzles, the radially contoured nozzle produced a uniform (or top hat) mean exit velocity profile that closely resembled those of the conventional smoothly contoured nozzles in previous studies [6], [7].

Table I lists the initial properties of the present jets, where δ_d and θ_m have been recalculated for "exit" $x/h = 0$ based on the experimental values at $x/h = 0.25$[1]. The orifice plate is found to produce the largest turbulence intensity in both its centerline (≈ 3.0%) and shear-layer (≈ 22%), which is reduced to ≈ 2.5%, and 17%, respectively, for the beveled-edge-orifice case. This observation is consistent with the vena contracta effect in orifice-jets, where the saddleback profiles poses larger regions

---

[1] The present exit boundary-layer characteristics (at x/h = 0) estimated from the values predicted by the "best-fit" curves of these properties measured at x/h = 0.25 reported by [4].

of mean velocity gradient, which in turn generate more turbulence. By contrast, the contoured nozzle produced the lowest turbulence intensity of ≈ 1.5% (centerline) and ≈ 4.0% within the shear-layers, which is associated with more laminar conditions of the initial jet.

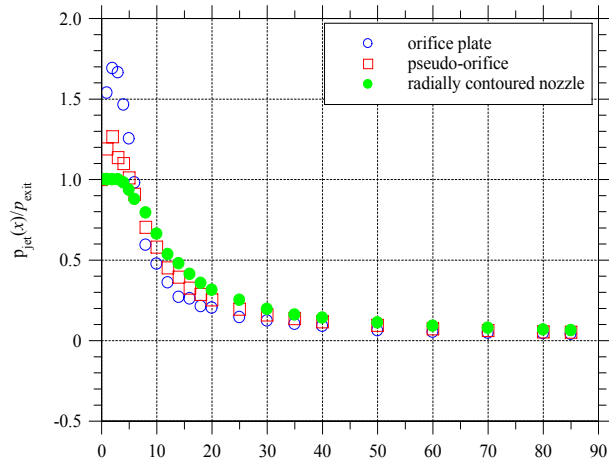Fig. 2 Total jet pressure variation on the jet centerline

The momentum (θ_m) and displacement thickness (δ_d) is higher for the contoured nozzle, which corresponds to a higher momentum-based Reynolds number, $Re_{\theta m} = U_b \theta_m / \upsilon$ for this nozzle. Of fundamental interest to the present investigation, and the results thereafter, is the turbulence Reynolds number, $Re_{u'}$, which is computed within the shear-layer of the initial jet. It is evidenced that the $Re_{u'}$ for the orifice is more than fivefold larger than the contoured nozzle, while that of the beveled-edge-orifice is fourfold larger. Such wide disparities clearly suggest that the initial flow structure of the orifice-jet significantly different, which is somewhat attributable to the vena contracta, and to the very thin initial boundary layer for this case. This accord with [12], [13] for round jets that also found thinner initial boundary layer with increased vorticity concentrated at the edge of the orifice compared to the contoured case.

B. Large-Scale Flow Statistics

Fig. 2 shows the centerline distributions of total jet pressure (P_{jet}/P_{exit}) for the orifice, beveled-edge-orifice and radially contoured nozzle. Here P_{exit} is the total jet pressure at $x = 0$ and P_{jet} is the corresponding value any x on the jet centerline, where $P = ½\rho U_{jet}^2$. In the near field ($x/h \approx 3$), the ratio P_{jet}/P_{exit} elevates rapidly for the two jets measured through the orifice-type nozzles. This yields a value of $P_{jet}/P_{exit} \approx 1.70$ and ≈1.30, for the orifice and beveled-edge-orifice nozzles, respectively. The spurt in the total jet pressure emanating from the orifice nozzle are primarily due to accelerated fluid brought about by the vena contracta, a common feature of jets issuing through orifice-kind geometries [10], [12], [13]. The contracted portion of the fluid is possibly triggered by rapid production of turbulence by the mean flow shear [16], [17] and thus implies

that near-field mixing among the three jets is highest in the orifice jet.

Furthermore, it is also deduced that a greater amount of the ambient fluid will generally be pumped into the orifice jet as result of the large differences in total jet pressure between the ambient and the jet [16], [17]. Based on the present data, the vena contracta region is pronounced when the nozzle geometry is much more abrupt. That is, as the geometry is modified from a beveled-edge-orifice to an orifice, the contracted portion of the jet fluid increases by ≈30%. However, unlike these two jets, the total jet pressure of the jet measured through the contoured nozzle is constant, with $P_{jet}/P_{exit} \approx 1$ for a downstream location $x \approx 5h$, which corresponds to the potential core of this jet.

Beyond the potential core and vena contractas, P_{jet}/P_{exit} declines rapidly for all three cases of investigation at least up to $x/h = 40$. This decline is perhaps supported by the production of turbulence through mean velocity shear [16]. However, the rate of decrease in total jet pressure for the orifice exceeds the rate of the other two jets, as the actual magnitude of P_{jet}/P_{exit} are relatively smaller at every downstream location. Based on this trend, it is deduced that the orifice-jet facilitates more rapid engulfment of the ambient fluid into its core, and could perhaps indicate more rapid mixing rates. For $x/h \geq 40$, the total jet pressure of all jets attains self-preservation, although the asymptotic values are some 50% higher for the flow through the contoured nozzle relative to orifice-type nozzles.

Fig. 3 (a) presents the streamwise evolution of normalized momentum thickness (θ_m/h) where $\theta_m(x)$ is obtained by applying numerical quadrature to the equation

$$\theta_m(x) = \int_{y=0}^{y=\infty} \left(\frac{U(x,y)}{U_c(x)} \right) \left(1 - \frac{U(x,y)}{U_c(x)} \right) dy \qquad (1)$$

That performs numerical integration of the mean velocity profile, $U(x, y)$ across the jet at any given x. Evidently, all data conform to a self-similar relationship of the form

$$\frac{\theta_m(x)}{h} = K_\theta \left(\frac{x - x_{01}}{h} \right) \qquad (2)$$

where K_θ (≡slope) and x_{01} (≡y-intercept) are some experimental constants. The linear rise of $\theta_m(x)$ with x accords with the previously reported trends of jet half-width by [10]. Comparatively, the jet issued through the contoured nozzle acquires smaller momentum thickness relative to the orifice case. This perhaps indicates lesser deficit in the shear-layer momentum of the former jet. For the orifice-case, the enhanced momentum thickness is consistent with the more rapid velocity decay and jet-spreading rates as reported previously [10] and the higher deficit in total jet pressure (Fig. 2). Indeed, the larger magnitude of $\theta_m(x)$ for the orifice appears to be associated with the vena contracta effect, which supposedly increases the instabilities within the jet's shear-layers. Since the shear-layer growth rates are proportional to $\theta_m(x)$, which in turn characterizes the scale of large eddies, it is deduced that the size

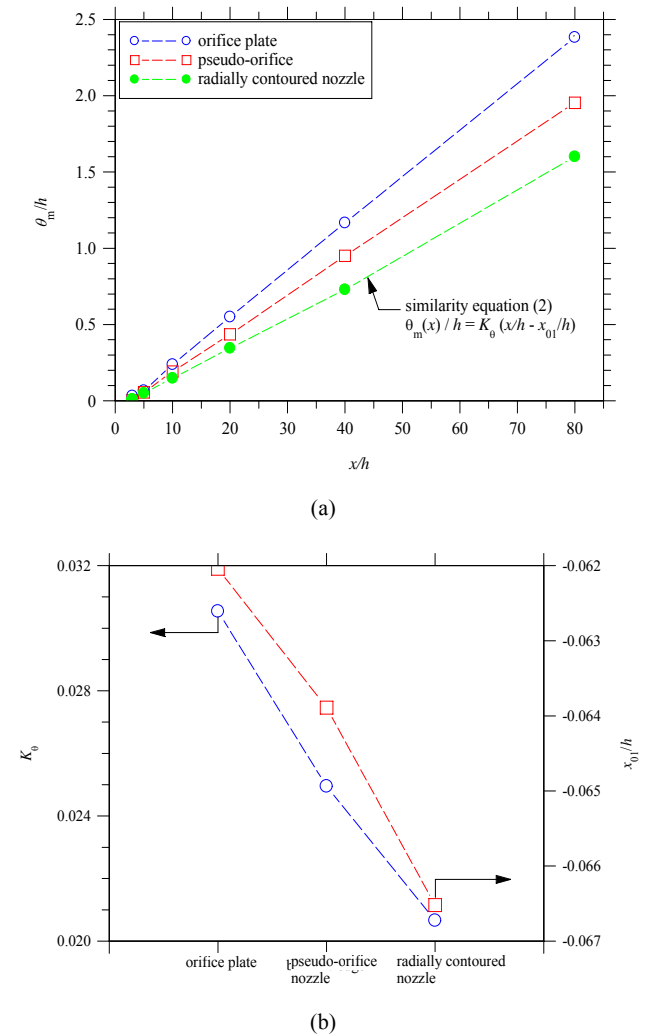of eddies are reduced for jets measured through the orifice-type nozzle.

(a)

(b)

Fig 3 (a) Streamwise growth of momentum thickness (θ_m); (b) Growth rate of large-scale, shear-layer given by $K_\theta = \frac{d\theta_m}{dx}$

In Fig. 3 (b), we compare the rate of change in $\theta_m(x)$ with x/h, where $K_\theta = d\theta_m/dx$ is the growth rate of the large-scale shear layer. Undoubtedly, K_θ decreases almost linearly with x for all cases of investigation. However, the jet emanating from the orifice plate exhibits ≈50% higher growth rates of shear-layer than one from the contoured nozzle. This consolidates the notion that the vena contracta for the orifice-jet plays a significant role in producing dynamical changes in the shear-layer development of the orifice jet. This also accords with well-known views [24], [25] that the momentum thickness plays a crucial role in jet spreading as well as governing the dynamics of large-scale coherent eddy structures.
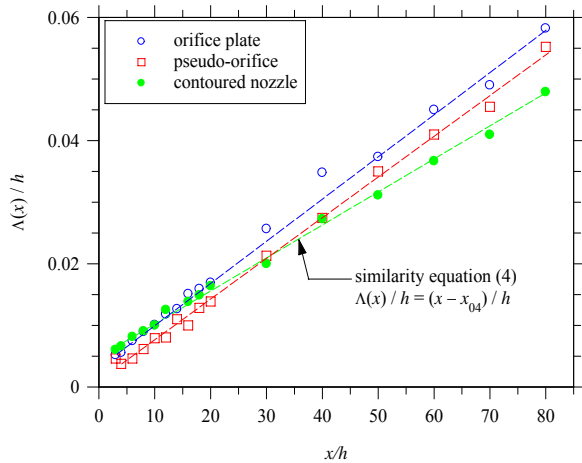
(a)
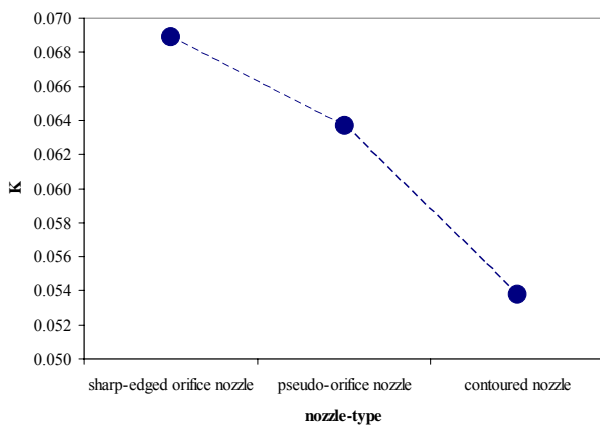
(b)
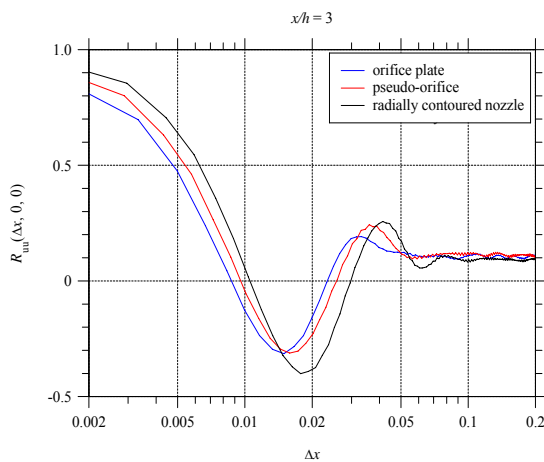
(c)

Fig. 4 (a) Integral length scales, $\Lambda(x)$ versus x/h (b) Growth rate of large-scale vortices, $K_\Lambda = \frac{d\Lambda}{dx}$ (c) Autocorrelation, R_{uu} at $x/h = 5$ in log-normal form

Next, we checked the autocorrelation function, $R_{uu}(\Delta x, 0, 0)$ of the fluctuating velocity (u) in order to estimate the size of large-scale eddy structures, sometimes termed as integral scales, $\Lambda(x)$. Note that the transformation $R_{uu}(\Delta x, 0, 0)$ is a convolution of the instantaneous velocity signal (u) at any given point (x_0) onto another point ($x_0 + \Delta x$). Fig. 4 (a) plots the present values of $\Lambda(x)$ all three jets, whereby

$$\Lambda = \int_{(x=0, R_{uu}=1)}^{(x=\Delta x, R_{uu}=0)} R_{uu}(\Delta x, 0, 0)\, d\Delta x \cdot \qquad (3)$$

In accordance with the trends in the downstream propagation and growth rates of large-scale eddies in turbulent plane jets [26], [27], $\Lambda(x)$ increases linearly with increasing x for all three cases. The variation of $\Lambda(x)$ with x accords with the similarity relationship

$$\frac{\Lambda(x)}{h} = K_\Lambda \left(\frac{x - x_{05}}{h} \right) = K_\Lambda\, \xi \qquad (4)$$

In (3), K_Λ ($\equiv$ slope) represents the growth rate of large-scale, coherent eddies, and x_{05} ($\equiv$ y-intercept) is the virtual origin. Beyond $x/h = 30$, the size of large-scale, coherent eddy structures embodied within the magnitudes of $\Lambda(x)$ are significantly smaller for the contoured nozzle relative to the orifice cases. Notably, the trend coincides with a higher Strouhal number of large-scale eddies for the former jet, as reported previously by [10]. In addition to the smaller eddy scales produces by the contoured nozzle, the growth rate of large-scale eddies as measured by the magnitude of K_Λ is $\approx 25\%$ lower, which is self-evident from Fig. 4 (b).

To corroborate notable disparities in large-scale coherent eddy sizes and their respective growth rates, Fig. 4 (c) displays a sample of the autocorrelation function, $R_{uu}(\Delta x, 0, 0)$ at $x/h = 3$ in the normal-log form. An immediate observation is that the area under the curve between the origin ($x = 0$) and Δx (where R_{uu} decays to the zero value on the abscissa), is indeed smaller for the orifice nozzle. The smaller integral hence confirms larger eddy sizes for this jet as demonstrated previously (Fig. 4 (a)). Furthermore, the R_{uu} also displays a meandering pattern for all three cases, although the troughs and peaks for $\Delta x \geq 0.01$ are obviously greater in amplitude for the orifice compared to the contoured nozzle.

Accordingly, we suspect that the jet generated from the orifice encompasses greater instabilities within the shear-layers; perhaps due to the relatively larger coherent eddies that are detected by the probe on the jet centerline (e.g. Fig. 4 (a)). One recalls that the orifice and beveled-edge-orifice nozzles produced a vena contracta around $x/h = 3$, so the rapid expansion of the jet along the lateral direction may create secondary instabilities that are responsible for the meandering patterns detected in the auto-correlation function. Accordingly, jets emanating from the orifice are more unstable than those from the contoured nozzle.

Fig. 5 presents the probability distribution function (pdf) of the fluctuating velocity (u) in the near field ($x/h = 5$), interaction

zone (x/h = 10), transition zone (x/h = 20) and self-preserving field (x/h = 80). All *pdfs* are normalized by $<u^2>^{1/2}$ and the Gaussian distribution $p(u_n) = 1/\sqrt{2\pi}\exp(-0.5\ln u_n^2)$ is shown. Despite some degree of departures that are deduced to be within the experimental uncertainties, the shapes of all *pdfs* in the near field closely resemble the Gaussian equation at x/h = 5. However, the general patterns of the distribution change in the interaction zone, where they exhibit shapes that do not converge to the Gaussian equation. Apparently, the *pdfs* are positively skewed for the orifice and negatively skewed for contoured case. That is, the mean skewness factors, $S_u = <u^3>/<u^2>^{3/2}$ of the velocity distributions are ≈+0.05 and -5, respectively.
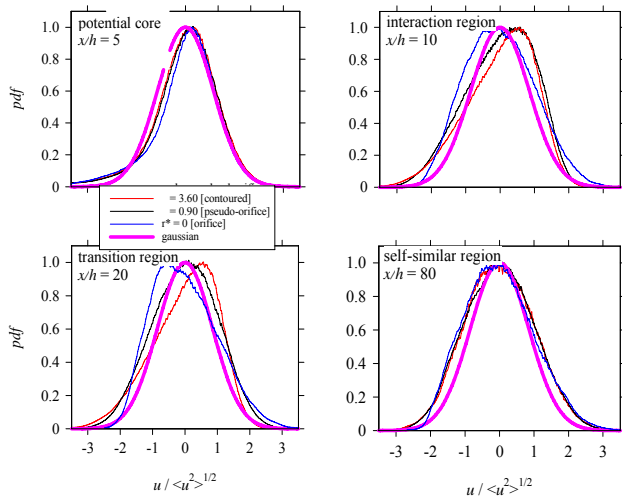

Fig. 5 The probability distribution functions of centerline velocity fluctuation measured in the potential core, interaction, transition and self-similar region

The distinctions in the *pdfs* at the onset of the interaction zone, where large-scale eddies revolve along the centerline to draw the ambient fluid [26], [27] into the jet imply substantial dependence of underlying shear-layer development on the nozzle geometry. That is, both jets produced from orifice nozzles preclude the ''potential core'' region (Fig. 2), which in turn facilitates more rapid growth of coherent eddy structures within their shear-layers (Fig. 3), and exhibit higher entrainment rates and the production of more coherent eddies. The *pdfs* in the interaction region (x/h = 20) register similar features with the orifice exhibiting more skewed distribution than the contoured nozzle, where the latter is closer to the Gaussian distribution. In the self-preserving field (x/h = 80), all *pdfs* converge to resemble the Gaussian profile, with subtle differences being within experimental uncertainties.

Fig. 6 (a) plots the one-dimensional streamwise turbulent kinetic energy, $E_k(x) = \frac{1}{2}<u_i><u_i>$, normalized by $U^2_c(x)$. Logarithmic ordinate and linear abscissa highlight the disparities in the magnitude of turbulent kinetic energy and their streamwise locations of asymptotic invariance. In accordance with previously reported trends of the centerline

turbulence intensity [10], there is a rapid increase in $E_k(x)/U^2_c(x)$ with increasing x for all three jets. This happens as the turbulence produced by mean velocity shear and the growth of shear-layers is advected by diffusion into the jet centreline. However, the actual values of the turbulent kinetic energy are discernibly different for the three types of jets throughout the measurement domain. It is also notable that, at x/h = 13, the orifice-jet produces a distinct "bump" in $E_k(x)$, which is absent in the other two jets. The notable distinctions in $E_k(x)$ are consistent with the different growth rates of shear-layers (Fig. 3) and the size of eddy structures (Fig. 4), and thus support greater anisotropy of the orifice-jet. In the self-preserving field, the orifice and beveled-edge-orifice jets sustain greater amount of turbulent kinetic energy than the jet issued from the contoured nozzle, which again is consistent with enhanced turbulence and anisotropic disorders fed into the near-field jet.
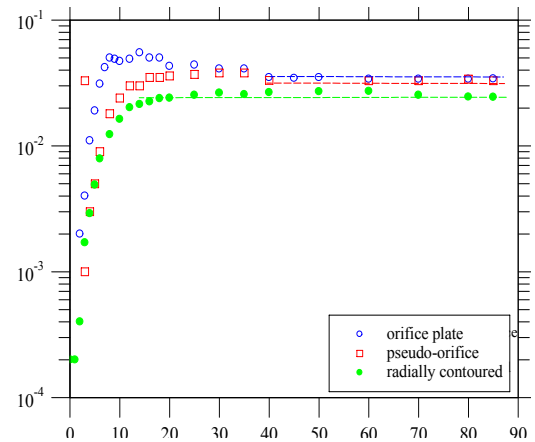

Fig. 6 The evolution of one-dimensional turbulent kinetic energy (E^*_k) on the jet centerline. Dashed lines show the asymptotic values

C. Frequency Analysis and Large-Scale Eddy Dynamics

Several investigations have consistently revealed that plane jets generate large-scale coherent eddy structures beyond the tip of the potential core, where the shear-layer begins breakdown and enlarge along the lateral direction [7], [28]–[30]. However, these eddy structures are predicted to depend on the nozzle geometry. For example, the symmetric mode eddy structures occur in a jet issuing from contracting nozzle, whose exit mean velocity is "top-hat" [28], [31], [32], while the anti-symmetric mode dominates the flow field of a channel or pipe jet whose mean exit velocity profile is of the power-law form [32]. Clearly, there is strong evidence that the nozzle geometry plays a pivotal role in moderating the dynamics of the large-scale flow of a turbulent plane jet.

To check the nature of the large-scale, coherent eddy structures emanating from the orifice and contoured nozzle, we computed the power spectra $\Phi_{E_k}(k)$ of the turbulent kinetic energy (E_k). $\Phi_{E_k}(k)$ is obtained by the Fourier transformation

of $E_k(x)$, so that $\int_0^\infty \Phi_{E_k}(k) = <u^2>$ is obtained at their respective Strouhal numbers, $St_h(x) = f(x)h/U_b$.

Fig. 7 plots the present values of $\Phi_{E_k}(k)$ against St_h for all three jets between $x/h = 0 - 10$. All spectra demonstrates that very close to the exit ($x/h \approx 0$), no fundamental peaks in $\Phi_{E_k}(k)$ are detected for any of the three cases. However, moving downstream to $x/h = 2$, well-defined spectral peaks appear in all three jets, although their height is somewhat reduced and their span on the abscissa is less broad for the orifice-jet relative to the other two cases. Between $x/h = 2 - 10$, the spectral peaks get smaller for all cases, and by $x/h = 10$, these have almost disappeared for the contoured nozzle, while the orifice still possess a weakly visible peak in $\Phi_{E_k}(k)$.
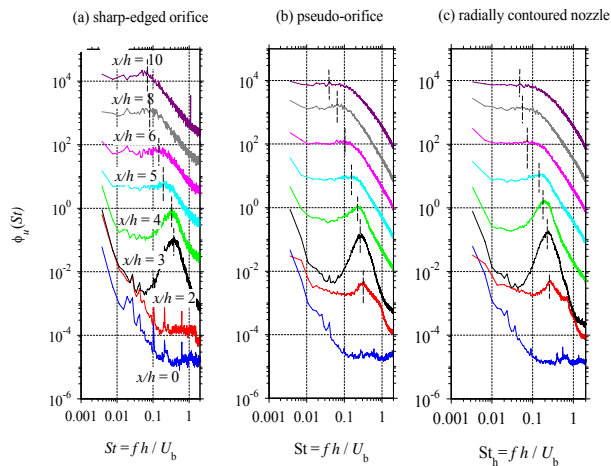

Fig. 7 Near-field evolutions of centerline velocity spectra, Φ_u. (a) orifice plate, (b) pseudo-orifice, and (c) radially contoured nozzle. Dashed lines show the fundamental modes of primary vortices

It is thus clear that the spectral characteristic of jets issuing from different nozzle geometries exhibit distinct features.

In general, the spectral peaks between $x/h = 2 - 10$ reflect the periodic passage of large-scale, coherent eddy structures, which are often produced beyond the tip of the potential core in turbulent plane jets. In this region, the main process involved is the roll-up of the unstable laminar shear-layers into the so-called "von-Karman vortex sheets" and the subsequent pairing, merging and interaction of large-scale vorticity of the opposite sign into both sides of the shear-layer [33]. Accordingly, the broad peaks in $\Phi_{E_k}(k)$ in the present investigation confirm the presence of regularly occurring periodic eddies in all three jets.

Similar features were depicted in flow visualizations of [23], who found streamwise eddy structures propagated between 0–4 nozzle-widths downstream. The early observations of [34] and [35] also reported symmetric eddy structures revolving on alternate sides of the shear layer, as they grew in size and paired up by coalescence with their adjacent counterparts [31]. The pairing process, self-induction and destruction continues until

all large-scale eddies are eventually broken down into the smallest (Kolmogorov) scale eddies.

Based on the present spectra, the visible peak at $x/h = 10$ for the orifice indicates a delay in the breakdown process or periodic passage of the large-scale coherent eddies for this jet. By contrast, the breakdown occurs more rapidly for the contoured nozzle, where spectral peaks have almost diminished by $x/h = 10$. The delay in the breakdown of eddies of the orifice stands somewhat at odds with lower dissipation rates and reduced size of small eddies for this jet, as shown later (Fig. 10 (a)-(b)). This deduction concurs with the independence of isotopic turbulent state from that of the large-scale turbulent state, as the basic premise for universal scaling is that effects of large-scale anisotropic forcings are eventually lost during the energy cascading process [36].

Indeed, this also accords with the local-isotropic hypothesis, which states that at sufficiently high Reynolds number the small-scale structures of turbulence are nominally independent of the large-scale structures and mean deformation rates [37]. For present cases, the delay in the breakdown of large-scale eddies is can be noted more clearly in Fig. 8, where the magnitude of the Strouhal number, $St_h(x)$ is greater for the orifice relative to the contoured nozzle at identical x-locations. Generally, $St_h(x)$ decreases with increasing x/h for all jets, and thus confirms the reduced importance of large-scale eddies at sufficiently great downstream distance.
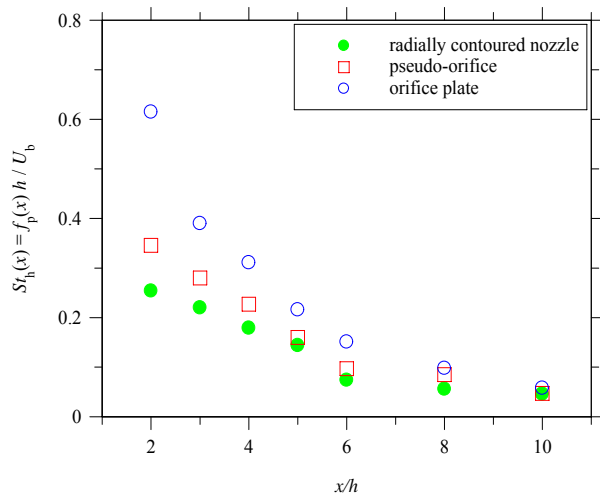

Fig. 8 Normalized Strouhal number of oscillation, $St_h(x)$ versus x/h

Now we examine the far-field spectra $\Phi_{E_k}(k)$ and their centerline evolutions. Fig. 9 present $\Phi_{E_k}(k)$ obtained between $x/h = 20 - 80$ for the orifice, beveled-edge-orifice and contoured nozzles, the linear ordinate and logarithmic abscissa are used. The presentation of the power spectra in the form $\Phi_{E_k} f / (\Phi_{E_k} f)_{max}$ versus $\log(f\, y_{0.5}(x)/U_c(x))$ identifies typical peaks in $\Phi_{E_k}(k)$ produced by the quasi-periodic passage of far-field coherent eddy structures [32]. In particular, the mean

square of the streamwise turbulence intensity $<u^2>$ is related to $\Phi_{E_k}(k)$ by

$$<u^2> = \int_0^\infty \Phi_{E_k}(f)df = \int_0^\infty f \Phi_{E_k}(f)d(\ln f) \qquad (6)$$

where the integral is directly proportional to the local streamwise energy of the fluctuating velocity, while the normal-logarithmic scaling of $\Phi_{E_k}f /(\Phi_{E_k}f)_{max}$ versus the local Strouhal number, $St_{y0.5}(x) = f\, y_{0.5}(x)/U_c(x)$ represents the contributions of the dominant frequencies to the spectral energy of each jet. It is observed that the spectra of the contoured nozzle converge nicely onto identical curves that resemble the normal distribution for $x/h \geq 20$, while those for the orifice plate converge for $x/h \geq 40$. This finding concurs with the similarity of the streamwise turbulent kinetic energy beyond these downstream location (Fig. 6) and previous observations of [32] who found good collapse of spectra when normalized by their local Strouhal numbers. Interestingly, the greater scatter in spectral data for the orifice-jet at $x/h = 20$ is quite expected, as the turbulent kinetic energy was not fully self-preserving until at least $x/h = 40$.
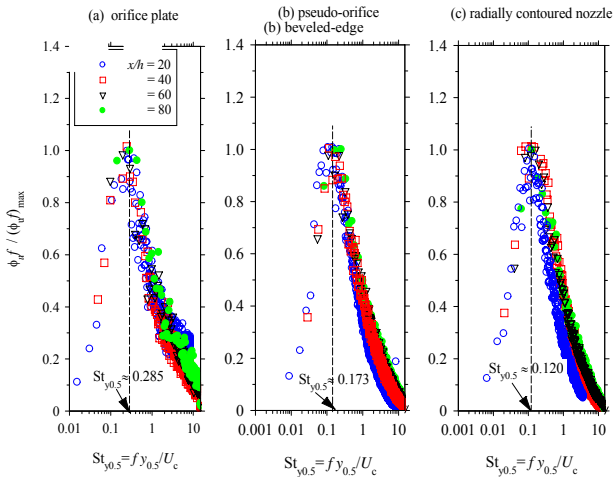

Fig. 9 Far-field evolutions of centreline velocity spectra, $\Phi_u f /(\Phi_u f)_{max}$. (a) orifice plate, (b) pseudo-orifice, (c) radially contoured nozzle

As shown by the dashed lines, the spectra are almost symmetric and centered around different values of $St_{y0.5}(x)$ on the abscissa. That is, the non-dimensionalization of the frequencies by local velocity half width, $y_{0.5}(x)$ and centerline mean velocity, $U_c(x)$ resulted in constant $St_{y0.5}(x)$ for the entire range of x/h. That is, the spectral peaks are centered around $St_{y0.5}(x) = 0.120 - 0.285$ depending on the nozzle geometry. The constancy of $St_{y0.5}(x)$ in the self-preserving field accords to investigations [32], [38], [39] for plane jet measurements.

Interestingly, the convergence of the far-field spectra onto single uniformly distributed curves when normalized by $y_{0.5}(x)$

and $U_c(x)$ indicates that the relative energy of the fluctuating velocity is independent of x in the self-preserving field. Furthermore, considering the constancy of $St_{y0.5}(x)$ and incorporating similarity relationships of the mean flow, $U_c(x) \sim x^{-1/2}$ and $y_{0.5}(x) \sim x$ into $St_{y0.5}(x) = f\, y_{0.5}(x)/U_c(x)$ yields $f \sim U_c^{-1/2}(x) \times y_{0.5}^{-1}(x) \equiv f \sim x^{-3/2}$. That the maximum turbulent kinetic energy in a given jet occurs at a constant Strouhal number when scaled with $y_{0.5}(x)$ and $U_c(x)$ accord with the similarity of the mean and the turbulent flow. However, significant disparities in the mean flow similarity (Figs. 2–3) and turbulence intensity (Fig. 6) between the orifice, beveled-edge-orifice and contoured nozzle seeds discernible spectral characteristics, and thus large-scale coherent eddy structures observed in the far-field jet.

From the same standpoint, the local Strouhal number being greater for the orifice compared to the contoured nozzle (0.285 *vs.* 0.120) agrees with the larger magnitude of turbulent kinetic energy in the self-preserving field (Fig. 6). This clearly shows that the higher passage frequency of the far-field, secondary coherent eddy structures is associated with the more energetic flow structures produced by the orifice, which again is self-evident (Fig. 9). In accordance with [38], the higher passage frequency of the orifice confirms greater "flapping motion" of this jet, which in the present investigation, is disparate, and indeed significantly enhanced for the jet issuing from the orifice relative to the contoured nozzle. The present finding agrees with those of [17] for their round jet measurements, where the sharp-edged orifice jet was found to be more "energetic" than the contoured nozzle jet.

The distinctly different features of underlying flow structure of the orifice-jet in both the near and far fields appear to have originated from the more complex flow at the nozzle exit. Recall that the initial structure of the orifice-jet is deduced to be more three-dimensional with a much larger turbulence Reynolds number than that from the contoured nozzle. This effect is perhaps associated to a vena contracta that generates strong recirculating separation regions both upstream and downstream of the nozzle exit. This observation contrasts the case of the contoured nozzle, where no upstream separation occurs [12]. Furthermore, the initial boundary layer of the beveled-edge-orifice is much thinner than that of the contoured nozzle (Table I), which also concurs with a greater instability of the initial jet. It thus follows that the three-dimensionality in the initial flow structure, which propagates downstream as also noted from spectral analysis is consistent with the greater flapping motion of the orifice-jet as previously stipulated by [38].

IV. CONCLUSIONS

The near and far flow field flows of plane jets measured at a Reynolds number of 18 000 issuing from a sharp-edged orifice, a beveled-edge and a radially contoured nozzle of aspect ratio 72 has been studied experimentally. The jet pressure deduced from centerline velocity measurements reveal a vena contracta for jets issuing from the orifice and beveled-edge-orifice

nozzles immediately downstream of the exit plane, which are larger in magnitude for the orifice case.

The streamwise distribution of momentum thickness and integral length scales increase linearly with x for all three jets, although the actual magnitudes are relatively larger for the orifice-jet. Accordingly, the growth rate of the shear layer and size of large-scale coherent eddies are substantially larger for the orifice compared to the contoured nozzle. These trends are confirmed by the autocorrelation coefficients of the streamwise fluctuating velocity which captured marked differences in the evolution of these jets. The autocorrelation functions of the orifice-jet exhibit greater meandering patterns and more rapid periodic oscillations that support higher instabilities within its shear-layer. These instabilities are perhaps associated with the vena contracta found in near-field region of the orifice-jets. The streamwise evolutions of turbulent kinetic energy in the near field incorporate a distinct "bump" around $x/h = 13$ for the orifice, which is not found in the jet emanating from the contoured nozzle. In the self-preserving field, the turbulent kinetic energy became asymptotically invariant for $x/h \geq 40$ and $x/h \geq 10$ for the orifice and contoured nozzles, respectively.

The near-field evolution of one-dimensional energy spectra confirms the presence of large-scale coherent structures in all jets. Importantly, the eddy structures are characterized by a greater passage frequency in the orifice jet flow. However, the Strouhal number of oscillation representing the passage frequency of large-scale eddy structures decreases with the increasing downstream evolution of all cases, although greater passage frequency is found for the orifice-jet when scaled by the local velocity half-width and mean velocity. This indicates that the far-field eddy structures are more presumably more "energetic" for the orifice jet flow. The present investigation also validates the similarity relationship, $St_{y0.5}(x) \sim x^{-1.5}$ to obey the requirements for self-preservation as shown by previous investigations [32] Finally, the observed discrepancies in large-and small-scale flow statistics thus reflect discernable flow structures in the near and far field of jets generated by the orifice, beveled-edge-orifice and radially contoured nozzle.

REFERENCES

[1] H. Schlichting, *Laminare strahlausbreitung*, ZAMM 13 260, 1933.
[2] S. Amiri, M. Sandberg, B. Moshfegh, "Effect of Cooling Loads on Warm Plane Air Jet", In Proc. *The 5th International Conference on Air Distribution in Rooms*, ROOMVENT '96. Yokohama, Japan, 1996.
[3] W. Quinn, "Development of a large-aspect ratio rectangular turbulent free jet", *AIAA J.*, vol 32(3), 1994.
[4] R.C. Deo, J. Mi, G.J. Nathan, "The influence of nozzle aspect ratio on plane jets", *Exp. Therm. Fluid. Sc.*, vol 31 (8) 825-833, 2007.
[5] G. Heskestad, "Hot-wire measurements in a plane turbulent jet", *Trans. ASME, J. Appl. Mech.*, vol 32, 721-734, 1965.
[6] L.J.S. Bradbury, "The structure of self-preserving turbulent planar jet", *J. Fluid Mech.*, vol 23, 31, 1965.
[7] E. Gutmark, I. Wygnanski, "The planar turbulent jet", *J. Fluid Mech.*, vol 73(3), 465–495, 1976.
[8] G.P Lemieux, P.H. Oosthuizen, "Experimental study of behaviour of planar turbulent jets at low Reynolds numbers", *AIAA J.* 1845–1846, 1985.
[9] G.P. Lemieux, P.H. Oosthuizen, "Experimental study of the behaviour of plane turbulent air jets at low Reynolds numbers", *17th Fluid Dynamics, Plasma Dynamics and Lasers Conference*, Paper AIAA-84-1661, Snow Mass/Co, USA, 1–6, 1984.
[10] R.C. Deo, J. Mi, G.J. Nathan, "The influence of nozzle-exit geometric profile on statistical properties of a turbulent plane jet," *Exp. Therm. Fluid Sci.* 32, 545, 2007.
[11] W.K. George, "Some new ideas for similarity of turbulent shear flows", In Proc. *ICHMT Symposium on Turbulence, Heat and Mass Transfer*, Lisbon, Portugal (1994), edited by K. Hanjalic and J. C. F. Pereira Begell, New York, 1995.
[12] J. Mi, G.J. Nathan, D.S. Nobes, "Mixing characteristics of axisymmetric free jets from a contoured nozzle, an orifice plate and a pipe", *J. Fluid. Eng.* 123, 878–883, 2001.
[13] J. Mi, D.S. Nobes, G.J. Nathan, "Influence of jet exit conditions on the passive scalar field of an axisymmetric free jet", *J. Fluid Mech.* 432, 91–125, 2001.
[14] R.C. Deo, "Experimental investigations of the influence of Reynolds number and boundary conditions on a plane air jet", *Ph.D. thesis*, The University of Adelaide, Australia, 2005. Available at Australian Digital Thesis Program, http://thesis.library.adelaide.edu.au/public/adt-SUA20051025.054550/index.html
[15] F.C. Lockwood, A. Moneib, Fluctuating Temperature Measurements in a Heated Round Free Jet, Combust. Sci. Technol., 22, 63–81, (1980).
[16] W.R. Quinn, "Upstream shaping effects on near field flow in round turbulent free jets". *Euro. J. Mech. B/Fluids*, 25 (3), 279-301, 2006.
[17] W.R. Quinn, "Experimental study of the near field and transition region of a free jet issuing from a sharp-edged elliptic orifice plate", *Euro. J. Mech. B/Fluids*, 26(4), 583-614, 2007.
[18] R. C. Deo, J. Mi, and G. J. Nathan, "Comparison of turbulent jets issuing from rectangular nozzles with and without sidewalls," *Experimental Thermal and Fluid Sciences*, vol 32, pp 596, 2007.
[19] H.H. Brunn, *Hot Wire Anemometry: Principles and Signal Analysis*, Oxford Press, (1995).
[20] P. Bradshaw, *An Introduction to Turbulence and Its Measurements*, Pergamon, 1971.
[21] F.H. Champagne, "The fine-scale structure of the turbulent velocity field", *J. Fluid Mech.* 86(1), 67–108, 1978.
[22] J. Tan-Atichat, W.K. George, S. Woodward, *Use of Data Acquisition and Processing: Handbook of Fluids and Fluids Engineering*, Vol. 3, Wiley, 1996.
[23] Y. Tsuchiya, C. Horikoshi, T. Sato, "On the spread of rectangular jets", *Exp. Fluids* 4, 197–204, 1985.
[24] C.M. Ho, E.J. Gutmark, "Vortex Induction and Mass Entrainment in a Small-Aspect Ratio Elliptic Jet", *J. Fluid Mech.*, 179, 383–405, 1987.
[25] H.S. Husain, A.K.M.F. Hussain, "Controlled excitation of elliptic jets", *Phys. Fluids*, vol 26, 2763, 1983.
[26] J.C. Mumford, "The structures of large eddies in fully developed shear flows. Part 1. The plane jet"., *J. Fluid Mech.*, vol 118, 241–268, 1982.
[27] A.K.M.F. Hussain, A.R. Clark, "Upstream influence on the near field of a planar turbulent jet", *Phys. Fluids*, vol 20(9), 1977.
[28] H. Sato, "The stability and transition of a two-dimensional jet", *J. Fluid Mech.*, vol 7, 53, 1960.
[29] F.O. Thomas, V.W. Goldschmidt, "Structural characteristics of a developing turbulent planar jet", *J. Fluid Mech.* 163, 227, (1986).
[30] P.R. Suresh, K. Srinivasan, T. Sundararajan, K. Das Sarit, "Reynolds number dependence of plane jet development in the transitional regime", *Phys. Fluids*, vol 20(4), 044105-12, 2008.
[31] D.O. Rockwell, W.O. Niccolls, "Natural breakdown of planar jets", *ASME J. Basic Eng.*, vol 94, 720, 1972.
[32] F.O. Thomas, K.M.K. Prakash, "An experimental investigation of the natural transition of an untuned planar jet", *Phys. Fluids*, vol A3, 90, 1991.
[33] A.K.M. F. Hussain, "Coherent structures and turbulence", *J. Fluid Mech.*, vol 173, 303, 1986.

[34] G.B. Brown, "On vortex motion in gaseous jets and origin of their sensitivity in sound", In Proc. *Phys. Soc.* London, vol 47, 703–732, 1935.

[35] G.S. Beavers, T.A. Wilson, "Vortex growth in jets", *J. Fluid Mech.* 44 (1) 97–112, 1970.

[36] L. Biferale, M. Vergassola, "Isotropy vs. anisotropy in small-scale turbulence", *Phys. Fluids*, vol 13, 2139, 2001.

[37] N. Kolmogorov, "Local structure of turbulence in an incompressible viscous fluid at very high Reynolds numbers", *Dokl. Akad. Nauk SSSR* 30, 299, 1941.

[38] R.A. Antonia, W.B. Browne, S. Rajagopalan, A.J. Chambers, "On organized motion of a turbulent planar jet", *J. Fluid Mech.*, vol 134, 49, 1983.

[39] R. C. Deo, J. Mi, and G. J. Nathan, "The influence of Reynolds number on a plane jet," *Physics of Fluids*, vol 20 (7), pp 075108-1, 2008.